INSTITUTE OF PHYSICS PUBLISHING JOURNAL OF PHYSICS D: APPLIED PHYSICS
J. Phys. D: Appl. Phys. **39** (2006) 3994–4000 doi:10.1088/0022-3727/39/18/011

Particle-in-cell simulation of beam extraction through a hole in contact with plasma

Sang Ki Nam, Demetre J Economou and Vincent M Donnelly

Plasma Processing Laboratory, Department of Chemical Engineering, University of Houston, Houston, TX 77204-4004, USA

Received 23 May 2006, in final form 26 July 2006
Published 1 September 2006
Online at stacks.iop.org/JPhysD/39/3994

Abstract
A particle-in-cell simulation of beam extraction through a hole in contact with plasma was developed. Particular emphasis was placed on plasma moulding over the hole, ion neutralization in high aspect ratio holes and the energy and angular distributions of the residual ions and fast neutrals in the beam downstream of the hole. When the sheath thickness is much smaller than the diameter of the hole, plasma moulding is severe, and the resulting ion and neutral beams are highly divergent. When the sheath thickness is much larger than the hole diameter, plasma moulding is weak, and collimated beams may be extracted. The angular distribution of fast neutrals peaks off axis, less so for smaller diameters and deep holes. Larger diameters and shallow holes (more plasma moulding) yield narrower ion energy distributions. The fast neutral energy distribution is predicted to be similar to that of ions, but it is shifted to lower energies.

1. Introduction

Beam extraction through a grid in contact with plasma finds applications in ion beam [1] as well as neutral beam sources [2–4]. For neutral beams, two cases are most frequently encountered: (a) an ion beam is extracted through a grid and the ions are neutralized downstream of the grid (by charge exchange with a neutral gas or by impinging the beam on a neutralizer plate) [4–6], or (b) ions are neutralized on the extraction grid itself by grazing angle collisions with the internal surfaces of the high aspect ratio holes of the grid [2, 3]. Neutral beams may be useful in mitigating charging damage in microelectronics fabrication [7, 8]. In any case, the flux, energy and angular distributions of the extracted beam (beam properties) are of primary importance for applications such as etching and deposition used in micro-fabrication [1]. Anisotropic etching of microelectronic materials, for example, requires a well-collimated beam. Beam properties can be critically affected by plasma moulding over the grid holes [9–11]. Plasma moulding refers to the ability of the plasma–sheath interface to 'contour' along the topography of surface features in contact with the plasma. In the case of plasma in contact with a grid, plasma moulding depends primarily on the diameter of the grid holes, D, as compared with the plasma sheath thickness, L_{sh}. When $L_{sh} \gg D$, the plasma–sheath interface (meniscus) is essentially planar as if the holes were not there (e.g. a solid wall). In the other extreme, $L_{sh} \ll D$, the plasma 'leaks' through the holes. In the intermediate case, $L_{sh} \sim D$, the plasma–sheath meniscus 'bends' gently over the holes [9]. The resulting beam should be highly directional (assuming no collisions in the sheath) when $L_{sh} \gg D$, and highly divergent when $L_{sh} \ll D$. On the other hand, the energy of the beam will depend on the potential difference between the plasma and the extraction grid.

In this work, a particle-in-cell (PIC) simulation was developed to study the angular and energy distributions of a beam extracted from a radio frequency (RF) plasma through a grid. A single hole in contact with the plasma was considered a simple geometry simulating a grid hole. Emphasis was placed on ion neutralization through high aspect ratio holes and the resulting neutral beam properties.

2. Simulation model

The two-dimensional axisymmetric (r, z) computational domain (figure 1) extended sufficiently far above the hole to include the sheath 'edge' (defined as the locus of points where the net charge density is 1% of the local ion density).

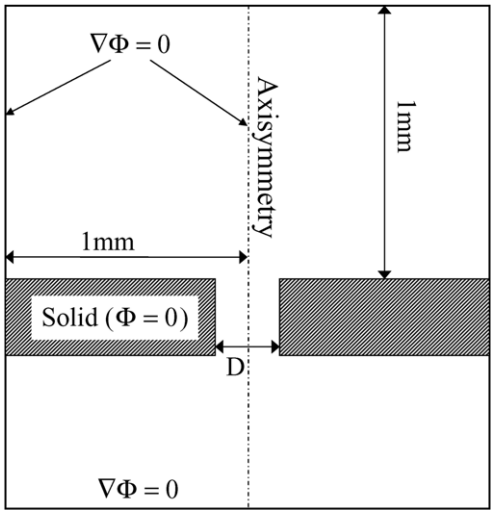

Figure 1. The computational domain consisted of an axisymmetric hole through a solid at ground potential, with the symmetry condition in the radial direction far from the hole. The ion density, electron temperature and plasma potential were specified at the top.

The ion density ($n_{i0} = 3 \times 10^{11}\,\mathrm{cm}^{-3}$), electron temperature ($T_\mathrm{e} = 6.8\,\mathrm{eV}$) and RF potential ($V_0 = 40 + 20\sin(2\pi f t)$, $f = 13.56\,\mathrm{MHz}$), were specified at the top boundary of the computational domain. These conditions correspond to one of the experiments described in [10]. The wall containing the hole was conductive and at ground potential ($V = 0$). A zero radial potential gradient was applied at the perimeter, and a zero axial potential gradient was applied at the bottom boundary of the computational domain.

The dynamics of a collisionless plasma can be described by the Vlasov equation in 6D phase space ($\vec{x}$, $\vec{v}$), where $\vec{x}$ and $\vec{v}$ are particle location and velocity, respectively

$$\frac{\partial f}{\partial t} + \vec{v}\cdot\frac{\partial f}{\partial \vec{x}} + \frac{\vec{F}}{m}\cdot\frac{\partial f}{\partial \vec{v}} = 0. \tag{1}$$

Here f is the particle distribution function, and $\vec{F} = q(\vec{E} + \vec{v}\times\vec{B})$ is the Lorenz force acting on a particle with charge q. The Lorenz force is generally obtained by solving Maxwell's equations. The PIC method tracks computational particles along the characteristics of the Vlasov equation with appropriate initial conditions. Particles are 'pushed' according to Newton's equation of motion,

$$\begin{aligned}\frac{\mathrm{d}\vec{x}}{\mathrm{d}t} &= \vec{v},\\ \frac{\mathrm{d}\vec{v}}{\mathrm{d}t} &= \frac{\vec{F}}{m}.\end{aligned} \tag{2}$$

At the end of the particle motion time step, the charge of each particle is distributed to the nodal points of the computational mesh using bilinear interpolation. Based on the resulting charge density, Poisson's equation is solved and the electric field is calculated on the nodal points. The electric field is then interpolated to the location of the particles using a bilinear function. The new electric field gives a new Lorentz force on the particles for the next motion time step. The cycle is repeated until a steady-state is reached and the statistics are adequate to calculate the particle distribution functions and the potential field.

Table 1. Geometry of the three holes studied.

Thickness of grid	254 μm	254 μm	254 μm
Diameter of hole	508 μm	127 μm	50.8 μm
Aspect ratio	1 : 2	2 : 1	5 : 1

An electropositive argon plasma containing a single ion species and electrons was simulated. Only the ions were followed by the PIC simulation. The electron density was assumed to be given by the Boltzmann relation (see [17, p 40]). The plasma sheath evolved self-consistently according to the specified conditions. Ions at the upper boundary of the computational domain were sampled from a drifting Maxwellian distribution using the acceptance–rejection method [12]. The ion temperature was 0.1 eV. An explicit time-centred leap frog method [13] was used for time integration, obeying the Courant condition, $(v\Delta t/\Delta x) < 1$, where v is the particle speed, and Δt and Δx are the time step and grid cell size, respectively. The pressure (5 mTorr) was sufficiently low for the ion flow to be collisionless. Particles injected at the top boundary of the computational domain were weighted according to their radial position so that a radially uniform ion flux was injected. Particles were pushed in a Cartesian coordinate system to avoid the singularity at $r = 0$. Particle distribution functions were collected at the bottom boundary of the computational domain. The Poisson equation was solved at each time step using a finite element method. Time marching continued until a periodic steady-state was achieved. The results shown below were obtained with 3×10^5 simulation particles. Energy conservation of the integration scheme was tested using cold ($T_i = 0$) ions in a two-dimensional DC field in the domain of figure 1. All particles collected at the bottom of the computational domain had the same energy indicating that there were no numerical artifacts.

3. Results and discussion

3.1. Potential and electric field distributions

Three cases were examined as shown in table 1. The hole diameter ranged from 50.8 to 127 to 508 μm. The wall thickness was 254 μm resulting in aspect ratios (thickness/diameter) of 5, 2 and 0.5, respectively. In all cases, results are shown after the periodic steady-state was achieved. This normally required some 100 RF cycles.

Figure 2 shows the time-average potential distribution for the three cases studied. The undisturbed sheath thickness (evaluated at the wall far away from the opening) was 130 μm under these conditions. Therefore the sheath is grossly perturbed in the case of the largest hole (figure 2(*a*)) but it is hardly affected in the case of the smallest hole (figure 2(*c*)). The potential profiles indicate the presence of strong lateral electric fields in the largest hole that can divert oncoming ions resulting in wide angular distributions. Also, a sizeable fraction of the ions can strike the sidewall and neutralize, despite the rather shallow (small aspect ratio) hole. The neutralized ions will emerge as fast neutrals with a wide angular distribution. The strength of the (time-average) horizontal component of the electric field is shown in figure 3. The electric

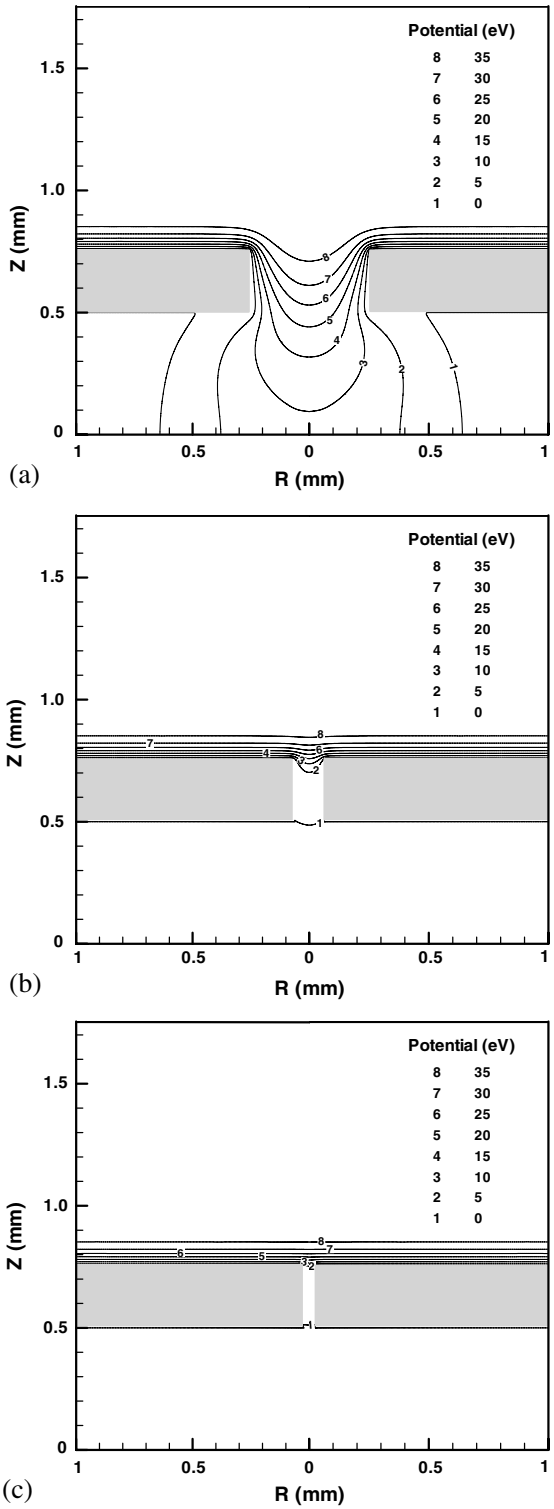

Figure 2. Time average potential distribution around holes with a diameter of 508 μm (*a*), 127 μm (*b*) and 50.8 μm (*c*). The undisturbed sheath thickness (on the wall away from the opening) was 130 μm. Ion flow was from top to bottom through a hole in a 254 μm thick solid grounded wall (represented by the grey area).

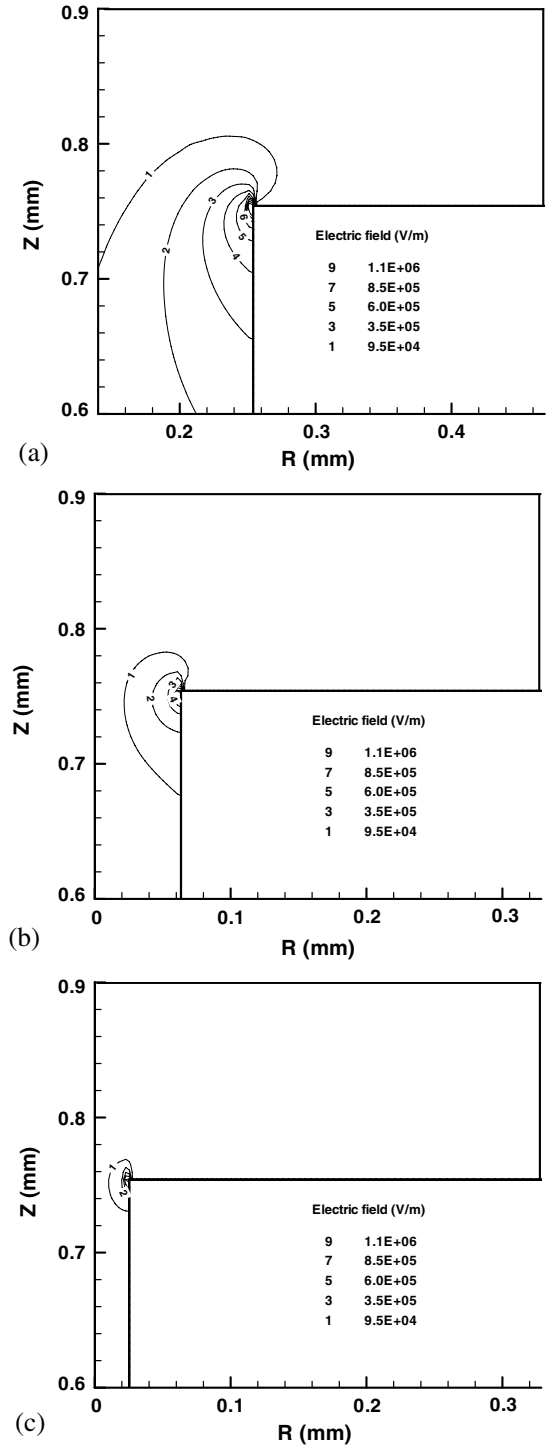

Figure 3. Magnitude of the time average horizontal component of the electric field for the conditions of figure 2.

field has a rather weak horizontal component in the smallest hole (figure 3(*c*)). In this case ions are accelerated mainly by the vertical component of the field. Thus, ions acquire a significant vertical velocity before arriving in the hole, where they 'feel' a horizontal field component (diverging field) for only a short time. Ions still have an angular distribution in the sheath, however, and a fraction of them can strike the sidewall to neutralize, exiting the hole as a fast neutral beam.

3.2. Ion energy and angular distributions

The energy distribution of the emerging ion beam is shown in figure 4. In the case of the largest hole, ions sample more

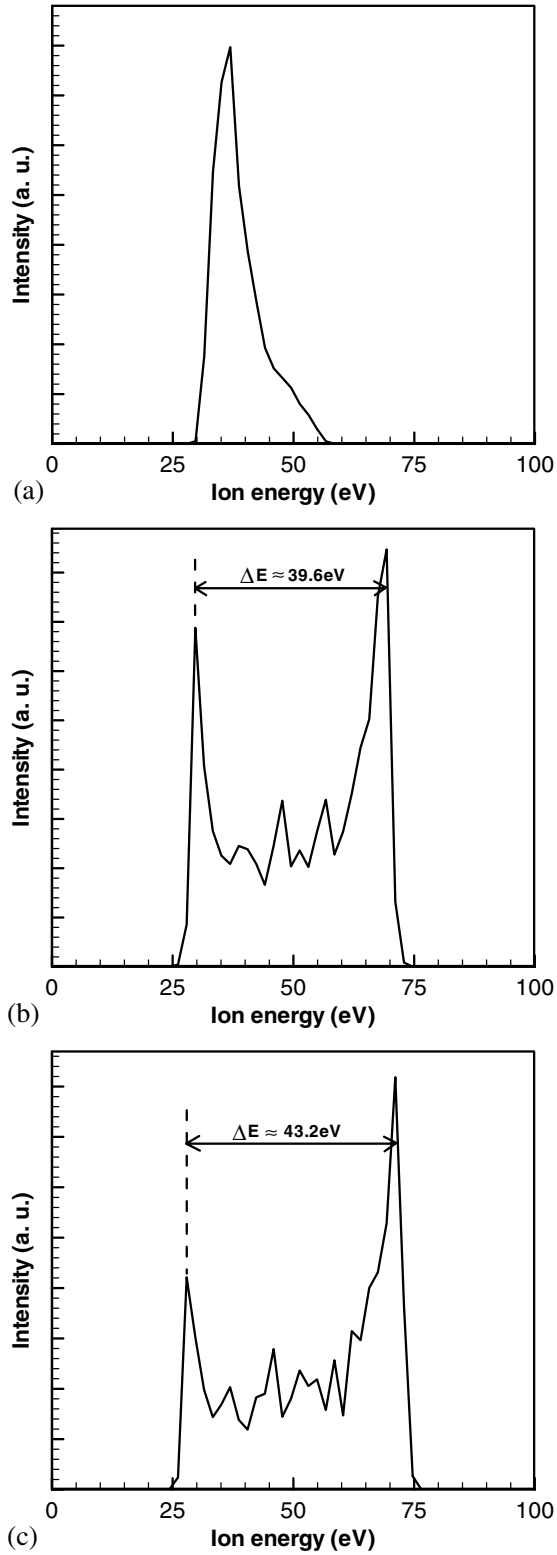

Figure 4. IED at the bottom of the computational domain for the conditions of figure 2.

of the average energy of the oscillating electric field, and the ion energy distribution (IED) exhibits a single peak. This case corresponds to an ion transit time in the sheath that is longer than the field period [15–17]. This is evident in figure 2(*a*) where the 'sheath' (region where potential gradients exist) extends all the way to the bottom of the domain. In contrast, in the case of the smallest hole, the transit time of ions through the sheath is shorter than the RF period. Thus ions feel more of the instantaneous sheath potential and the IED has the characteristic double-peak shape (figure 4(*c*)). The IED of the intermediate size hole (figure 4(*b*)) also shows two peaks but the energy separation of these peaks is smaller (39.6 V compared with 43.2 V in figure 4(*c*)).

The ion angular distributions (IAD) are shown in figure 5. Large diameters and shallow holes give wide angular distributions (figure 5(*a*)), while small diameters and deep holes give narrow distributions (figure 5(*c*)). The half-width-at-half-maximum (HWHM) of the distributions for 508 μm, 127 μm and 50.8 μm diameter holes are 47.5°, 11.7° and 4.3°, respectively. The HWHM of the IED on a flat wall (no plasma moulding) is 1.6° under these conditions.

3.3. Comparison with experiments

Figure 6 shows a comparison of simulation predictions with data from [10]. The sharp drop off in the measured IAD, beyond 30°, was due to beam shadowing in the experimental apparatus. Otherwise a wide angular distribution was observed as seen in the simulations. The measured IED had a single peak with a shape quite similar to the simulated IED. The width of the IED, however, was smaller in the simulation probably because of underestimating the sheath potential used in the simulation.

3.4. Fast neutral energy and angular distributions

Ions that encounter the wall were assumed to neutralize with 100% probability [17]. Ions would neutralize by, for example, an Auger process, a distance of the order of ∼1 Å from the surface. A simple surface interaction model was used, assuming specular scattering with an energy exchange given by [18]

$$\sqrt{\frac{\varepsilon_r}{\varepsilon_i}} = \left(\frac{\mu}{\mu+1}\right)^2 \left(\cos\chi_{1/2} + \sqrt{\frac{1}{\mu^2} - \sin^2\chi_{1/2}}\right)^2,$$
$$\chi_{1/2} = \frac{\pi}{2} - \vartheta_i, \qquad \mu = \frac{m_{\mathrm{Ar}}}{m_{\mathrm{wall}}}. \tag{3}$$

Here ε_i and ε_r are kinetic energy of the incident and reflected atom, respectively, θ_i is the incident angle and m_{Ar} and m_{wall} are the mass of the argon atom and the wall material atom, respectively.

This expression corresponds to two successive binary collisions of the impinging ion (actually a neutral by the time it encounters the surface) with surface atoms. Specular scattering may be a reasonable approximation for grazing angle collisions with atomically flat surfaces. However, it is expected to be a poor approximation for non-grazing angle collisions especially of real (rough) surfaces.

Figure 7 shows the fast neutral energy distributions (NED) for the 127 and 50.8 μm diameter holes. The corresponding IED are also shown. The NED is similar to the IED except for a shift to lower energies due to collisions with surface atoms. The energy loss is larger in the case of the 127 μm diameter hole because of the smaller angle (with respect to the surface normal) at which ions strike the surface. This is

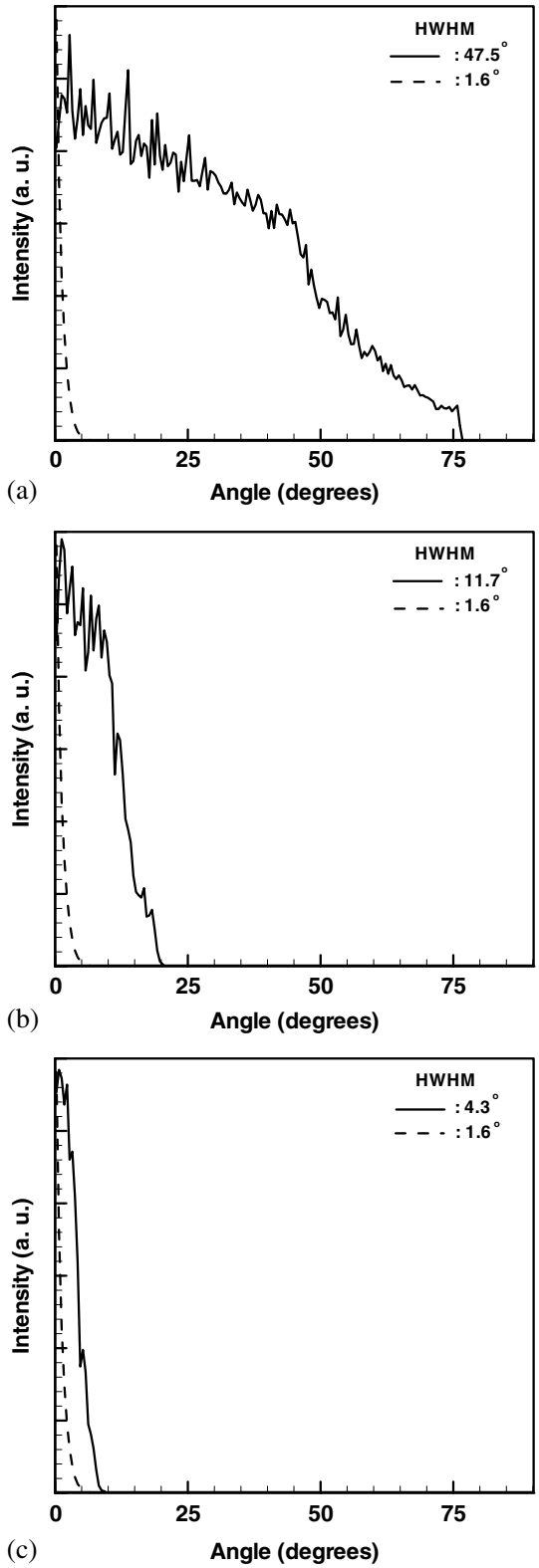

Figure 5. IAD at the bottom of the computational domain (——) for the conditions of figure 2. The HWHM of the IAD on the wall for an undisturbed sheath (away from the opening) is 1.6° (- - - -).

a result of more plasma moulding and a stronger component of the horizontal electric field for the larger hole (compare figure 3(*b*) with 3(*c*)). The area under the curves give the relative flux of neutrals compared with the ions. Clearly, most

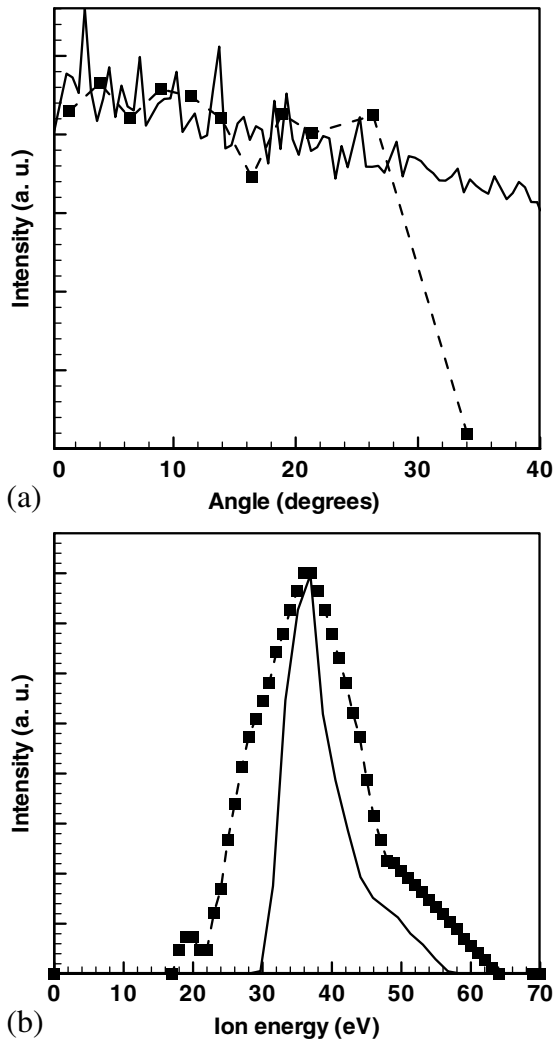

Figure 6. Comparison of simulation predictions (——) with experimental data (· · · · · ·) from [10], for a hole diameter of 508 μm. Due to shadowing in the experimental apparatus, there is a cut-off in the measured IAD around 30°.

of the oncoming ions strike the internal walls of the holes and are neutralized. The fast neutral angular distributions (NAD) for the 127 and 50.8 μm hole diameters are shown in figure 8. The angular distributions of the residual ions are also shown. The NADs peak off normal as dictated by the geometry of specular reflection. The 'hole' in the centre of the NAD (around zero angle) is larger for the 127 μm diameter hole, reflecting the wider IAD obtained in that hole. Otherwise the NADs are as wide as the parent IADs. Figure 8 suggests that smaller diameters and deeper holes give narrower NAD with a smaller 'hole' in the centre of the distribution.

For the three cases of table 1 studied, the fraction of ions entering the hole that were neutralized (struck the sidewall) was 51%, 85%, and 87% for the 254 μm, 127 μm and 50.8 μm hole diameter, respectively. Since the 50.8 μm hole has a much higher aspect ratio, compared with the 127 μm hole, one would expect more than 2% difference in the degree of neutralization between these holes. However, plasma moulding over the 50.8 μm hole is weaker, resulting in higher ion directionality, thus compensating for the aspect ratio difference.

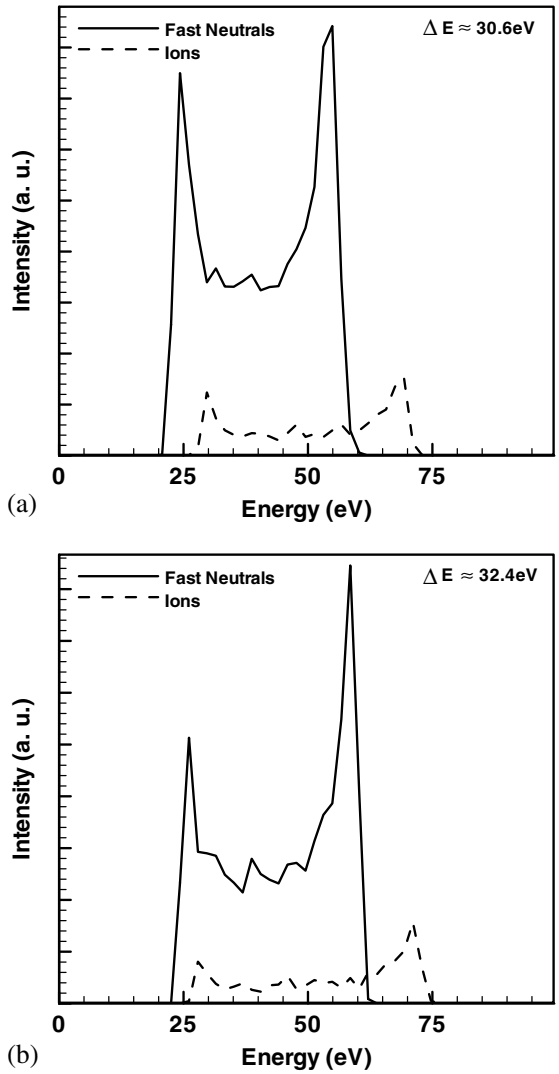

Figure 7. Fast NED at the bottom of the computational domain (——) for a hole diameter of 127 μm (*a*) and 50.8 μm (*b*). The corresponding IED are shown as dashed lines.

4. Summary

A PIC simulation was developed to study the effect of plasma moulding on the energy and angular distributions of beams extracted from a hole in contact with the plasma. Emphasis was placed on ion neutralization by surface collision with the internal walls of high aspect ratio holes. This is one method of generating a fast neutral beam that can find applications in charge-free microelectronics manufacturing. When the sheath thickness is much smaller than the diameter of the hole, plasma moulding is severe, the plasma–sheath interface 'dips' inside the hole, and the resulting ion and neutral beams are highly divergent. When the sheath thickness is much larger than the hole diameter, plasma moulding is weak, and collimated beams may be extracted. The angular distribution of fast neutrals peaks off axis, less so for smaller diameter and deep holes. Larger diameter and shallow holes (more plasma moulding) yield narrower IED. The fast NED is similar to that of ions, but it is shifted to lower energies as ions lose energy in collisions with the wall.

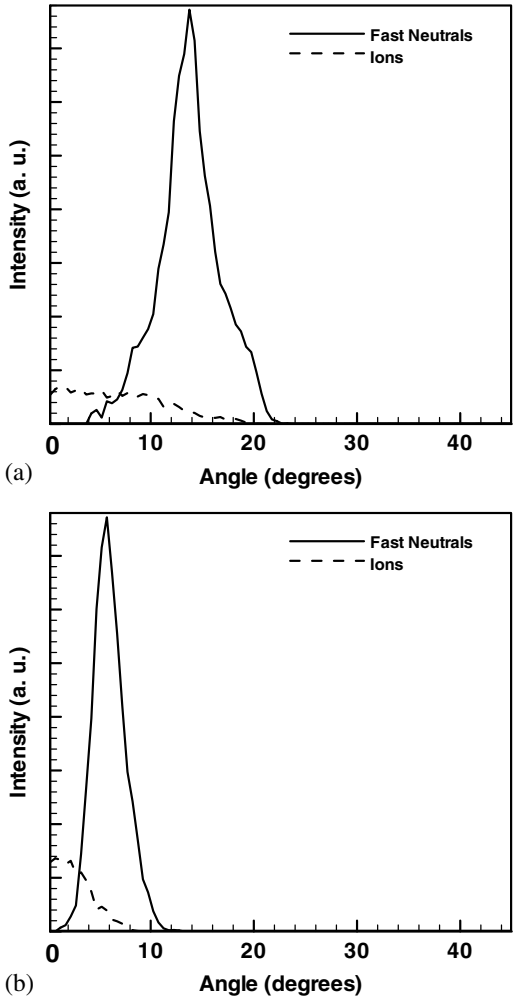

Figure 8. Fast NAD at the bottom of the computational domain (——) for a hole diameter of 127 μm (*a*) and 50.8 μm (*b*). The corresponding IAD are shown as dashed lines.

Acknowledgments

Financial support from the National Science Foundation (CTS 0072854 and MII-0303790) and the Texas Advanced Technology Program is gratefully acknowledged.

References

[1] Rossnagel S M, Cuomo J J and Westwood W D (ed) 1990 *Handbook of Plasma Processing Technology* (Park Ridge, NJ: Noyes)
[2] Panda S, Economou D J and Chen L 2001 *J. Vac. Sci. Technol.* A **19** 398
[3] Samukawa S, Sakamoto K and Ichiki K 2002 *J. Vac. Sci. Technol.* A **20** 1566
[4] Kim S J, Lee H J, Yeom G Y and Lee J K 2004 *Japan. J. Appl. Phys* **43** 7261
[5] Nichols C A and Manos D M 1996 *J. Appl. Phys* **80** 2643
[6] Cuthbertson J W, Motley R W and Langer W D 1992 *Rev. Sci. Instrum* **63** 5279
[7] Economou D J and Alkire R C 1988 *J. Electrochem. Soc.* **135** 941
[8] Hwang G S and Giapis K P 1997 *J. Vac. Sci. Technol.* B **15** 70
Kinoshita T, Hane M and McVittie J P 1996 *J. Vac. Sci. Technol.* B **14** 560

[9] Kim D and Economou D J 2002 *IEEE Trans. Plasma Sci.* **30** 2048
[10] Kim C-K and Economou D J 2002 *J. Appl. Phys.* **91** 2594
[11] Kim D and Economou D J 2003 *J. Vac. Sci. Technol.* B **21** 1248
[12] Bird G A 1994 *Molecular Gas Dynamics and the Direct Simulation of Gas Flows* (Oxford: Clarendon Press)
[13] Birdsall C K 1991 *IEEE Trans. Plasma Sci.* **19** 65
[14] Miller P A and Riley M E 1997 *J. Appl. Phys.* **82** 3689
[15] Panagopoulos T and Economou D J 1999 *J. Appl. Phys.* **85** 3435
[16] Edelberg E K, Perry A, Benjamin N and Aydil E S 1999 *J. Vac. Sci. Technol.* A **17** 506
[17] Lieberman M A and Lichtenberg A J 1994 *Principles of Plasma Discharges and Materials Processing* (New York: Wiley)
[18] Helmer B A and Graves D B 1998 *J. Vac. Sci. Technol.* A **16** 3502